High-speed enhanced K-edge angiography utilizing cerium plasma x-ray generator

Eiichi Sato, MEMBER SPIE
Iwate Medical University
Department of Physics
Morioka 020-0015, Japan
E-mail: dresato@iwate-med.ac.jp

Etsuro Tanaka
Tokyo University of Agriculture
Department of Nutritional Science
Faculty of Applied Bioscience
Setagaya-ku 156-8502, Japan

Hidezo Mori
National Cardiovascular Center Research Institute
Department of Cardiac Physiology
Osaka 565-8565, Japan

Toshiaki Kawai, MEMBER SPIE
Hamamatsu Photonics K. K.
Electron Tube Division #2
Iwata-gun 438-0193, Japan

Shigehiro Sato
Iwate Medical University
Department of Microbiology
School of Medicine
Morioka 020-8505, Japan

Kazuyoshi Takayama, MEMBER SPIE
Tohoku University
Shock Wave Research Center
Institute of Fluid Science
Sendai 980-8577, Japan

Abstract. The cerium target plasma flash x-ray generator is useful to perform high-speed enhanced K-edge angiography using cone beams, because K-series characteristic x-rays from the cerium target are absorbed effectively by iodine-based contrast mediums. In the plasma generator, a 200-nF condenser is charged up to 60 kV by a power supply, and flash x-rays are produced by the discharging. The x-ray tube is a demountable triode with a trigger electrode, and the turbomolecular pump evacuates air from the tube with a pressure of approximately 1 mPa. Target evaporation leads to the formation of weakly ionized linear plasma, consisting of cerium ions and electrons, around the target, and intense flash x-rays are produced. At a charging voltage of 55 kV, the maximum tube voltage is almost equal to the charging voltage of the main condenser, and the maximum current is approximately 20 kA. When the charging voltage is increased, weakly ionized cerium plasma forms, and the K-series characteristic x-ray intensities increase. The x-ray pulse widths are about 500 ns, and the time-integrated x-ray intensity has a value of about 40 μC/kg at 1.0 m from the x-ray source with a charging voltage of 55 kV. In the angiography, we employ a filmless computed radiography (CR) system and iodine-based microspheres.

[DOI: 10.1117/1.1882372]

Subject terms: plasma x-ray; cerium target; weakly ionized cerium plasma; characteristic x-ray; K-edge angiography.

Paper 040183 received Mar. 26, 2004; revised manuscript received Sep. 9, 2004; accepted for publication Oct. 25, 2004; published online Apr. 6, 2005. This paper is a revision of a paper presented at the SPIE conference on Ultrahigh- and High-Speed Photography, Photonics, and Videography, Aug. 2003, San Diego, California. The paper presented there appears (unrefereed) in SPIE Proceedings Vol. 5210.

1 Introduction

Flash x-rays are useful to perform high-speed radiography, and various generators have been developed to correspond to specific radiographic objectives.[1–5] In the cases of multishot and cine radiographies, we have developed several different repetitive-flash[6–10] and stroboscopic x-ray generators.[11–17] Although most flash x-ray generators have cold-cathode tubes, the stroboscopic generators utilize hot-cathode tubes.

In conjunction with single crystals, synchrotrons generate monochromatic x-rays. These rays play important roles in parallel radiography and have been employed to perform high-contrast K-edge angiography[18] and x-ray phase imaging.[19,20] However, it is difficult to obtain sufficient machine times for various research projects, including medical applications.

As for angiography using iodine-based contrast mediums, K-series characteristic x-rays of cerium are extremely useful, since the rays are absorbed easily by iodine. In particular, since fairly intense and sharp characteristic x-rays have been produced from weakly ionized linear plasmas[21–24] of nickel, copper, and molybdenum, the development of a cerium-target x-ray tube for angiography is highly desirable.

In this research, we developed a single flash x-ray generator with a cerium-target plasma tube and performed a preliminary study on weakly ionized cerium plasma angiography.

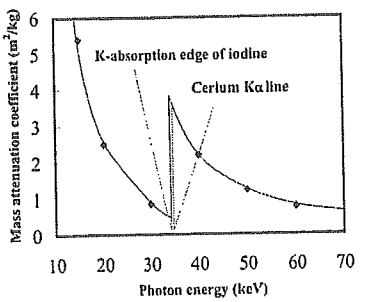

Fig. 1 Relation between mass attenuation coefficient of iodine and average photon energy of cerium Kα lines.

0091-3286/2005/$22.00 © 2005 SPIE

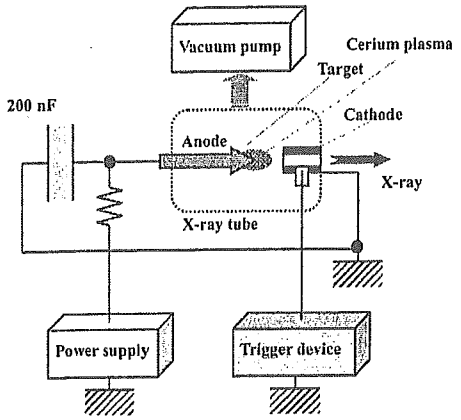

Fig. 2 Block diagram of high intensity plasma flash x-ray generator.

2 Principle of K-Edge Angiography

Figure 1 shows the mass attenuation coefficients of iodine at the selected energies; the coefficient curve is discontinuous at the iodine K-edge. The average photon energy of the cerium Kα lines is shown just above the iodine K-edge. Cerium is a rare earth element and has a high reactivity; however, the average photon energy of Kα lines is 34.566 keV, and iodine contrast mediums with a K-absorption edge of 33.155 keV absorb the lines easily. Therefore, blood vessels were observed with high contrasts.

3 Generator

3.1 *High-Voltage Circuit*

Figure 2 shows a block diagram of a high-intensity plasma flash x-ray generator. This generator consists of the following essential components: a high-voltage power supply, a high-voltage condenser with a capacity of about 200 nF, a turbomolecular pump, a krytron pulse generator as a trigger device, and a flash x-ray tube. The high-voltage main condenser is charged up to 60 kV by the power supply, and

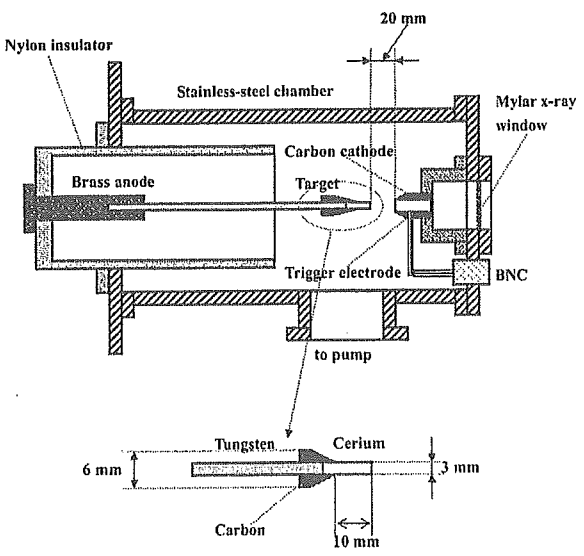

Fig. 3 Schematic drawing of flash x-ray tube.

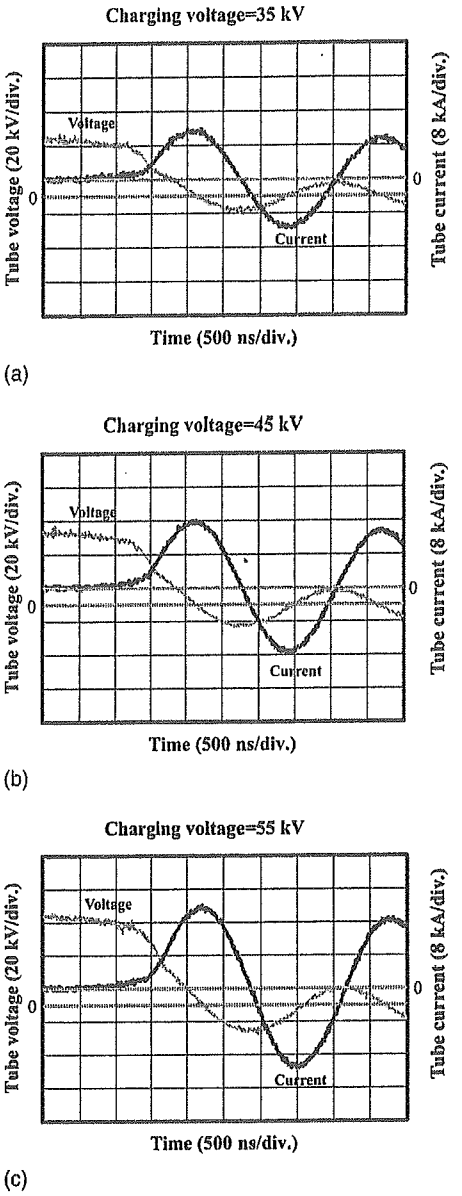

Fig. 4 Tube voltages and currents with charging voltage of (a) 35, (b) 45, and (c) 55 kV.

electric charges in the condenser are discharged to the tube after triggering the cathode electrode by the trigger device. The plasma flash x-rays are then produced.

3.2 *X-Ray Tube*

The x-ray tube is a demountable cold-cathode triode that is connected to the turbomolecular pump with a pressure of approximately 1 mPa (Fig. 3). This tube consists of the following major parts: a hollow cylindrical carbon cathode with a bore diameter of 10.0 mm, a trigger electrode made from a copper wire, a stainless-steel vacuum chamber, a nylon insulator, a polyethylene terephthalate (Mylar) x-ray window of 0.25 mm, and a rod-shaped cerium target of 3.0 mm in diameter. The target tip is embedded in the carbon rod to absorb the characteristic x-rays of carbon by the window. The distance between the target and cathode electrodes is approximately 20 mm, and the trigger electrode is

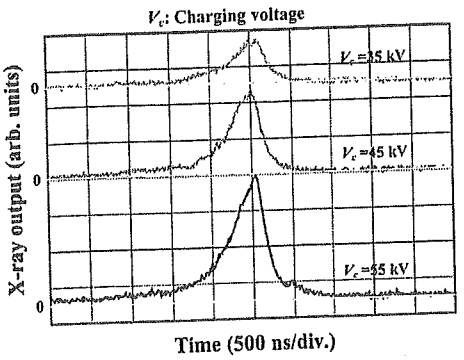

Fig. 5 X-ray outputs at indicated conditions.

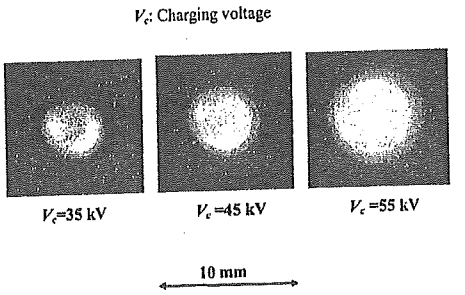

Fig. 6 Images of plasma x-ray source.

set in the cathode electrode. As electron beams from the cathode electrode are roughly converged to the target by an electric field in the tube, the weakly ionized plasma, which consists of cerium ions and electrons, forms around the target by evaporating.

4 Characteristics

4.1 *Tube Voltage and Current*

Tube voltage and current were measured by a high-voltage divider with an input impedance of 1 GΩ and a current transformer, respectively. Figure 4 shows the time relation between the tube voltage and current. At the indicated charging voltages, they roughly displayed damped oscillations. When the charging voltage was increased, both the maximum tube voltage and current increased. At a charging voltage of 55 kV, the maximum tube voltage was almost equal to the charging voltage of the main condenser, and the maximum tube current was about 20 kA.

4.2 *X-Ray Output*

An x-ray output pulse was detected using a combination of a plastic scintillator and a photomultiplier. The x-ray pulse height substantially increased with corresponding increases in the charging voltage (Fig. 5). The x-ray pulse widths were about 500 ns, and the time-integrated x-ray intensity measured by a thermoluminescence dosimeter (Kyokko TLD Reader 1500 utilizing MSO-S elements without energy compensation) had a value of about 40 μC/kg at 1.0 m from the x-ray source with a charging voltage of 55 kV.

4.3 *X-Ray Source*

To measure images of the plasma x-ray source, we employed a pinhole camera with a hole diameter of 100 μm (Fig. 6). When the charging voltage was increased, the plasma x-ray source grew, and both spot dimension and intensity increased. Because the x-ray intensity is the highest at the center of the spot, both the dimension and intensity decreased according to both increases in the thickness of a filter for absorbing x-rays and decreases in the pinhole diameter.

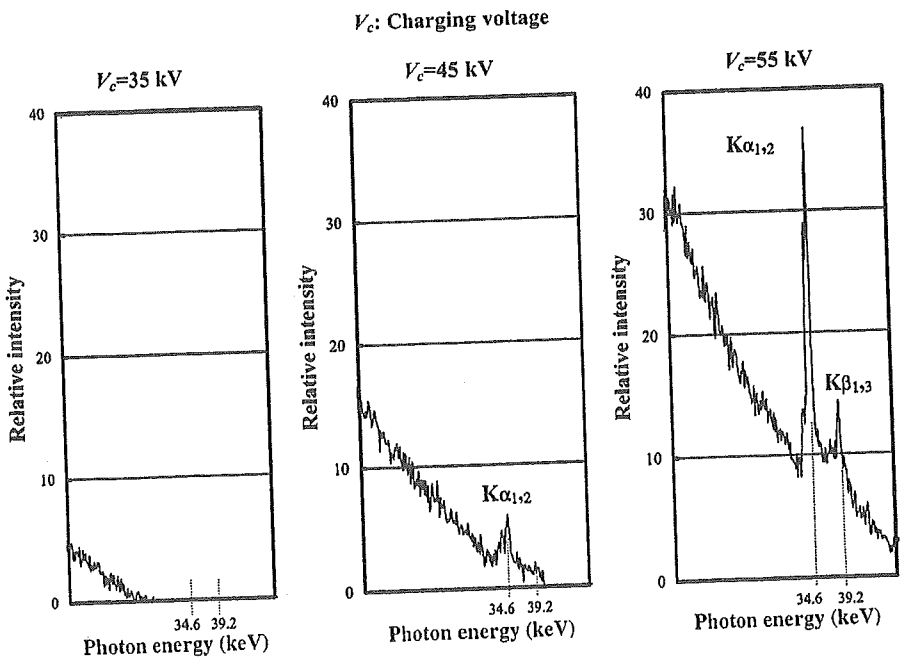

Fig. 7 X-ray spectra from weakly ionized cerium plasma.

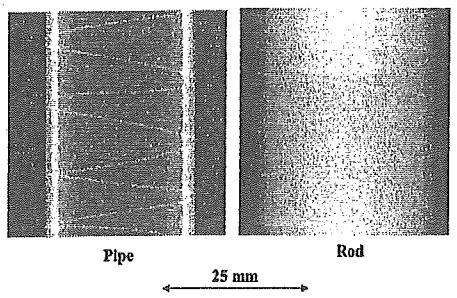

Fig. 8 Radiograms of tungsten wires of 50 μm in diameter coiled around pipe and rod made of PMMA.

4.4 *X-Ray Spectra*

X-ray spectra from the plasma source were measured by a transmission-type spectrometer with a lithium fluoride curved crystal of 0.5 mm in thickness. The spectra were taken by a computed radiography (CR) system[25] (Konica Regius 150) having a wide dynamic range, and relative x-ray intensity was calculated from Dicom digital data. Figure 7 shows measured spectra from the cerium target. In this experiment, although we observed both the bremsstrahlung and characteristic x-rays, we could not observe characteristic x-rays with a charging voltage of 35 kV, because the critical excitation energy is 40.3 keV. Both intensities increased substantially with increases in the charging voltage.

5 Angiography

The plasma angiography was performed by the CR system without using a monochromatic filter, and the distance between the x-ray source and the imaging plate was 1.2 m.

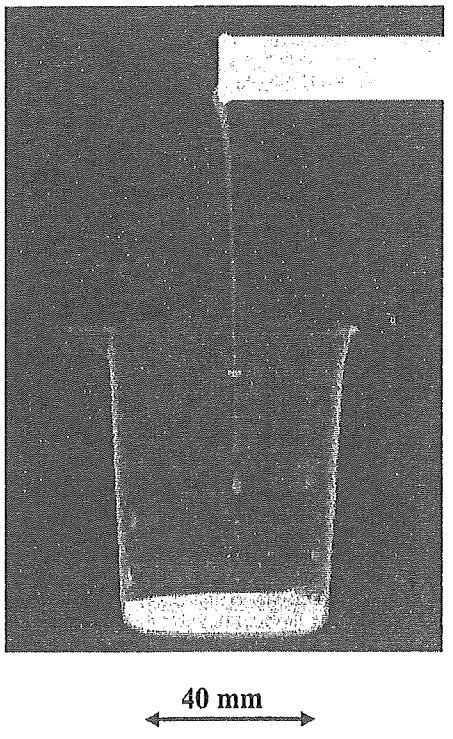

Fig. 9 Radiogram of water falling into a polypropylene beaker from a glass test tube.

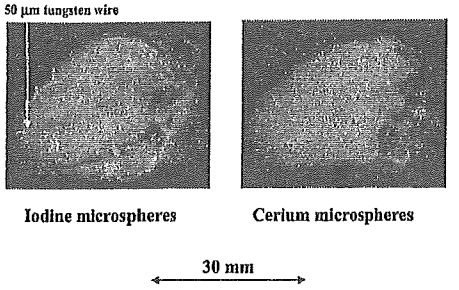

Fig. 10 Angiograms of rabbit hearts using iodine and cerium microspheres.

Subsequently, in angiography testing, we usually employ nonliving animal phantoms using microspheres.

First, rough measurements of image resolution were made using wires. Figure 8 shows radiograms of 50-μm-diam tungsten wires coiled around a pipe, and a rod made of polymethyl methacrylate (PMMA) with a charging voltage of 55 kV. Although the image contrast increased using the pipe, 50-μm-diam wires could be observed.

The image of water falling into a polypropylene beaker from a glass test tube is shown in Fig. 9. This image was taken with a charging voltage of 55 kV, with the slight addition of an iodine-based contrast medium. Because the x-ray duration was about 1 μs, the stop-motion image of water could be obtained.

Angiograms of rabbit hearts are shown in Fig. 10. These two images were obtained using iodine and cerium microspheres of 15 μm, respectively, with a charging voltage of 55 kV. In cases where the cerium spheres were employed, the coronary arteries were barely visible. Figure 11 shows an angiogram of the external ear of a rabbit using iodine spheres with a charging voltage of 55 kV, and fine blood vessels of about 50 μm are visible. In angiography of a larger heart extracted from a dog, using iodine spheres, a PMMA plate was set in front of a heart facing x-ray source, and image contrast of coronary arteries improved with increases in the plate thickness (Fig. 12).

6 Discussion

In an earlier experiment using a copper target,[24] bremsstrahlung x-rays were hardly observed at all, and we confirmed the irradiation of fairly clean K-series characteristic x-rays such as lasers. In the present work, although we confirmed intense characteristic x-rays with a higher charging voltage, bremsstrahlung x-rays were detected, since the bremsstrahlung intensity is proportional to the atomic num-

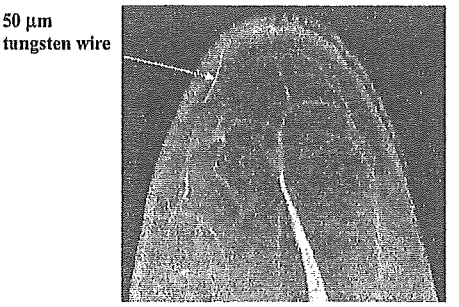

Fig. 11 Angiograms of external ear of rabbit.

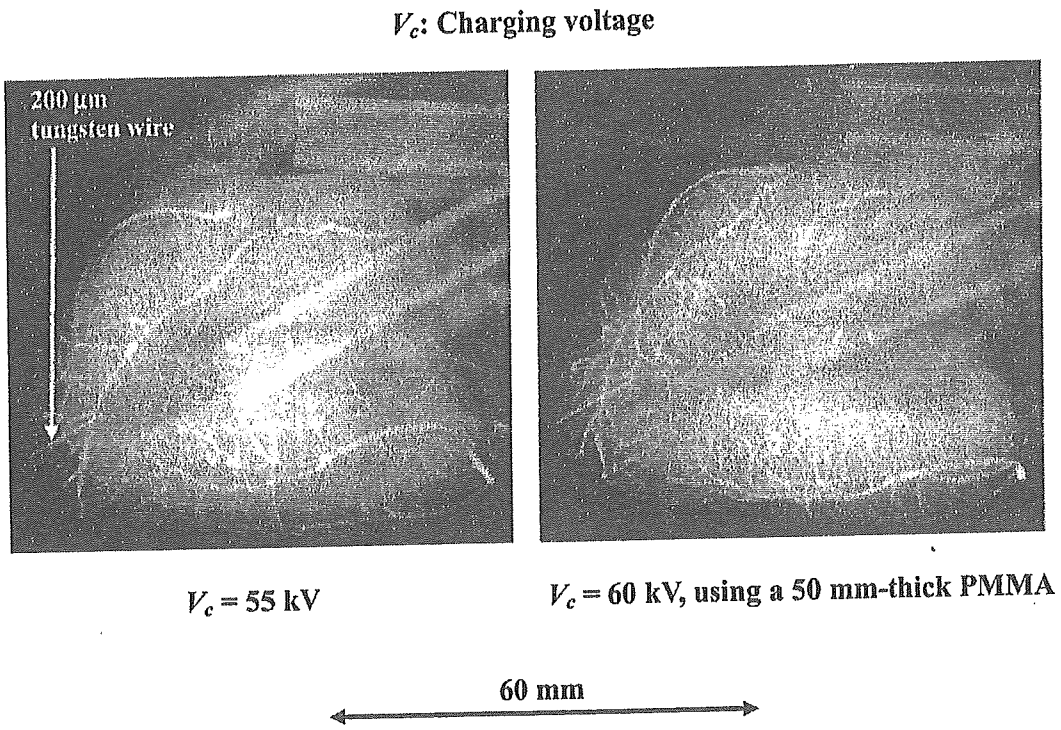

Fig. 12 Angiograms of extracted heart of dog.

ber of the target element, and high-photon-energy bremsstrahlung x-rays are not absorbed effectively in the plasma. Therefore, the condenser charging voltage should be raised as high as possible to increase the characteristic x-ray intensity. To decrease emission of bremsstrahlung x-rays from the carbon target holder, the target length should also be set as long as possible. Next, since the spheres easily transmit bremsstrahlung x-rays with energies lower than the edge, it is important that the rays be absorbed as much as possible before angiography to increase the image contrast.

In this research, we obtained sufficient x-ray intensity per pulse for CR radiography, and the generator produced high-dose-rate plasma x-rays of approximately 80 C/kg·s at 1.0 m with a charging voltage of 55 kV. In addition, because the x-ray intensity increases with increases in the electrostatic energy in the main discharge condenser, the flash x-rays from weakly ionized linear cerium plasma can be employed to perform high-speed angiography for cardiovascular disease.

Acknowledgments

This work was supported by Grants-in-Aid for Scientific Research (13470154, 13877114, and 16591222) and Advanced Medical Scientific Research from MECSST; Health and Labor Sciences Research Grants (RAMT-nano-001, RHGTEFB-genome-005, and RHGTEFB-saisei-003); and grants from Keiryo Research Foundation, The Promotion and Mutual Aid Corporation for Private Schools of Japan, Japan Science and Technology Agency (JST), and New Energy and Industrial Technology Development Organization (NEDO, Industrial Technology Research Grant Program in '03).

References

1. A. Mattsson, "Some characteristics of a 600 kV flash x-ray tube," *Phys. Scr.* **5**, 99–102 (1972).
2. R. Germer, "X-ray flash techniques," *J. Phys. E* **12**, 336–350 (1979).
3. E. Sato, H. Isobe, and F. Hoshino, "High intensity flash x-ray apparatus for biomedical radiography," *Rev. Sci. Instrum.* **57**, 1399–1408 (1986).
4. E. Sato, M. Sagae, K. Takahashi, T. Oizumi, H. Ojima, K. Takayama, Y. Tamakawa, T. Yanagisawa, A. Fujiwara, and K. Mitoya, "High-speed soft x-ray generators in biomedicine," *Proc. SPIE* **2513**, 649–667 (1994).
5. E. Sato, M. Sagae, A. Shikoda, K. Takahashi, T. Oizumi, M. Yamamoto, A. Takabe, K. Sakamaki, Y. Hayasi, H. Ojima, K. Takayama, and Y. Tamakawa, "High-speed soft x-ray techniques," *Proc. SPIE* **2869**, 937–955 (1996).
6. E. Sato, S. Kimura, S. Kawasaki, H. Isobe, K. Takahashi, Y. Tamakawa, and T. Yanagisawa, "Repetitive flash x-ray generator utilizing a simple diode with a new type of energy-selective function," *Rev. Sci. Instrum.* **61**, 2343–2348 (1990).
7. S. Kimura, E. Sato, M. Sagae, A. Shikoda, T. Oizumi, K. Takahashi, Y. Tamakawa, and T. Yanagisawa, "Disk-cathode flash x-ray tube driven by a repetitive two-stage Marx pulser," *Med. Biol. Eng. Comput.* **31**, S37–S43 (1993).
8. A. Shikoda, E. Sato, M. Sagae, T. Oizumi, Y. Tamakawa, and T. Yanagisawa, "Repetitive flash x-ray generator having a high-durability diode driven by a two-cable-type line pulser," *Rev. Sci. Instrum.* **65**, 850–856 (1994).
9. E. Sato, K. Takahashi, M. Sagae, S. Kimura, T. Oizumi, Y. Hayasi, Y. Tamakawa, and T. Yanagisawa, "Sub-kilohertz flash x-ray generator utilizing a glass-enclosed cold-cathode triode," *Med. Biol. Eng. Comput.* **32**, 289–294 (1994).
10. K. Takahashi, E. Sato, M. Sagae, T. Oizumi, Y. Tamakawa, and T. Yanagisawa, "Fundamental study on a long-duration flash x-ray generator with a surface-discharge triode," *Jpn. J. Appl. Phys.* **33**, 4146–4151 (1994).
11. E. Sato, A. Shikoda, S. Kimura, M. Sagae, H. Isobe, Y. Tamakawa, and T. Yanagisawa, "Kilohertz-range flash x-ray generator utilizing a triode in conjunction with an extremely hot cathode," *Rev. Sci. Instrum.* **62**, 2115–2120 (1991).
12. E. Sato, M. Sagae, K. Takahashi, A. Shikoda, T. Oizumi, Y. Hayasi, Y. Tamakawa, and T. Yanagisawa, "10 kHz microsecond pulsed x-ray generator utilizing a hot-cathode triode with variable durations for biomedical radiography," *Med. Biol. Eng. Comput.* **32**, 295–301 (1994).
13. E. Sato, T. Ichimaru, T. Usuki, K. Sato, H. Ojima, K. Takayama, H.

Ido, K. Sakamaki, and Y. Tamakawa, "Condenser-discharge stroboscopic x-ray generator SX-C98," *Proc. SPIE* **3516**, 618–625 (1998).
14. E. Sato, T. Ichimaru, H. Ojima, K. Takayama, H. Ido, and Y. Tamakawa, "Characteristics of the kilohertz-range harder stroboscopic x-ray generator and applications," *Proc. SPIE* **3771**, 12–21 (1999).
15. E. Sato, T. Ichimaru, H. Obara, M. Zuguchi, H. Mori, E. Tanaka, T. Usuki, K. Sato, H. Ojima, K. Takayama, K. Sakamaki, and Y. Tamakawa, "Condenser-discharge stroboscopic x-ray generator for medical radiography," *Proc. SPIE* **4183**, 383–393 (2000).
16. E. Sato, H. Ojima, K. Takayama, M. Matsumasa, H. Obara, M. Zuguchi, T. Usuki, K. Sato, K. Sakamaki, and Y. Tamakawa, "Observation of cavitation bubble cloud using a stroboscopic x-ray generator," *Proc. SPIE* **4183**, 394–404 (2000).
17. E. Sato, Y. Hayasi, and Y. Tamakawa, "Recent stroboscopic x-ray generators and their applications to high-speed radiography," *Ann. Rep. Iwate Med. Univ. Lib. Arts and Sci.* **35**, 1–11 (2000).
18. H. Mori, K. Hyodo, E. Tanaka, M. U. Mohammed, A. Yamakawa, Y. Shinozaki, H. Nakazawa, Y. Tanaka, T. Sekka, Y. Iwata, S. Honda, K. Umetani, H. Ueki, T. Yokoyama, K. Tanioka, M. Kubota, H. Hosaka, N. Ishizawa, and M. Ando, "Small-vessel radiography in situ with monochromatic synchrotoron radiation," *Radiology* **201**, 173–177 (1996).
19. T. J. Davis, D. Gao, T. E. Gureyev, A. W. Stevenson, and S. W. Wilkins, "Phase-contrast imaging of weakly absorbing materials using hard x-rays," *Nature (London)* **373**, 595–597 (1995).
20. A. Momose, T. Takeda, Y. Itai, and K. Hirano, "Phase-contrast x-ray computed tomography for observing biological soft tissues," *Nat. Med.* **2**, 473–475 (1996).
21. E. Sato, Y. Hayasi, E. Tanaka, H. Mori, T. Kawai, T. Usuki, K. Sato, H. Obara, T. Ichimaru, K. Takayama, H. Ido, and Y. Tamakawa, "Quasi-monochromatic radiography using a high-intensity quasi-x-ray laser generator," *Proc. SPIE* **4682**, 538–548 (2002).
22. E. Sato, Y. Hayasi, R. Germer, E. Tanaka, H. Mori, T. Kawai, H. Obara, T. Ichimaru, K. Takayama, and H. Ido, "Intense characteristic x-ray irradiation from weakly ionized linear plasma and applications," *Jpn. J. Med. Imag. Inform. Sci.* **20**, 148–155 (2003).
23. E. Sato, Y. Hayasi, R. Germer, E. Tanaka, H. Mori, T. Kawai, H. Obara, T. Ichimaru, K. Takayama, and H. Ido, "Irradiation of intense characteristic x-rays from weakly ionized linear molybdenum plasma," *Jpn. J. Med. Phys.* **23**, 123–131 (2003).
24. E. Sato, Y. Hayasi, R. Germer, E. Tanaka, H. Mori, T. Kawai, T. Ichimaru, K. Takayama, and Hideaki Ido, "Quasi-monochromatic flash x-ray generator utilizing weakly ionized linear copper plasma," *Rev. Sci. Instrum.* **74**, 5236–5240 (2003).
25. E. Sato, K. Sato, and Y. Tamakawa, "Film-less computed radiography system for high-speed Imaging," *Ann. Rep. Iwate Med. Univ. Sch. Lib. Arts Sci.* **35**, 13–23 (2000).

Elichi Sato received his BS, MS, and PhD in applied physics from Tohoku Gakuin University, Sendai, Japan, in 1979, 1982, and 1987, respectively. From 1982, he was an assistant in the Department of Physics, and became an associate professor in 1986. Since 2004, he has been a professor of physics at Iwate Medical University. He has written some 400 publications and delivered some 200 international presentations concerning x-rays. His research interests include soft flash x-ray generators, quasi-x-ray laser generators, and high-speed radiography. In 2000 he received the Schardin Gold Medal from the German Physical Society, and in 2003 he received the Takayama Award (Gold Medal) from the Japan Society of High Speed Photography and Photonics.

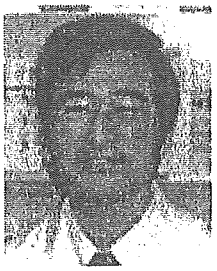

Etsuro Tanaka received his MD and PhD degrees in medicine from Kumamoto University, Japan, in 1980 and 1986, respectively. He worked on medical image processing in the Department of Physiology, Tokai University, Japan, from 1988 to 2003. He is currently a professor in the Department of Nutritional Sciences, Tokyo University of Agriculture, Japan. His research interests include medical image processing, human physiology, and clinical nutrition.

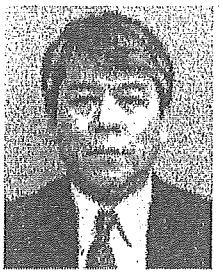

Hidezo Mori received a medical degree from Keio University School of Medicine, Tokyo, Japan, in 1977, and also a PhD from the Post Graduate School, Keio University School of Medicine. Now he is the director of the Department of Cardiac Physiology at the National Cardiovascular Center, Suita, Japan. His primary research interests are regenerative therapy in cardiovascular disease, microcirculation, and medical applications of structural biology.

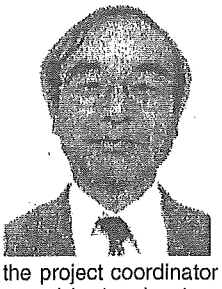

Toshiaki Kawai received the BS degree in precision mechanics and the MS degree in electronic engineering from Shizuoka University, Hamamatsu, Japan, in 1964 and 1974, respectively. In 1974, he joined the Hamamatsu Photonics K.K., where he worked on research and development of solid-state infrared detectors, and then from 1978 to 1981 engaged in research work on the NEA cold cathode for application to imaging camera tubes. He is now the project coordinator of the Electron Tube Division #2 and is engaged in the development and manufacturing of imaging devices and x-ray equipment. He is a member of the Japan Radioisotope Association and the Institute of Image Information and Television Engineers of Japan.

Shigehiro Sato received his MD degree from Iwate Medical University in 1980. He worked for the laboratory of the Division of Pediatric Infectious Diseases at Johns Hopkins Hospital from 1985 to 1989. He is currently a professor in the Department of Microbiology at Iwate Medical University. His research interests include central nervous system damage caused by Vero toxin, a cell culture system for vaccine development, and microangiography.

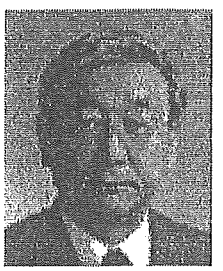

Kazuyoshi Takayama received his BS degree from Nagoya Institute of Technology in 1962. In 1970, he received his PhD in mechanical engineering from Tohoku University. Since 1986, he has been a director (professor) of the Shock Wave Research Center, Institute of Fluid Science, Tohoku University. His research interests include various shock wave phenomena, high-speed photography, and flash radiography. He has received seven awards including the coveted Ernst Mach Medal in 2000.

Clean monochromatic x-ray irradiation from weakly ionized linear copper plasma

Eiichi Sato, MEMBER SPIE
Iwate Medical University
Department of Physics
Morioka 020-0015, Japan
E-mail: dresato@iwate-med.ac.jp

Etsuro Tanaka
Tokyo University of Agriculture
Department of Nutritional Science
Faculty of Applied Bioscience
Setagaya-ku 156-8502, Japan

Hidezo Mori
National Cardiovascular Center Research Institute
Department of Cardiac Physiology
Osaka 565-8565, Japan

Toshiaki Kawai, MEMBER SPIE
Hamamatsu Photonics K.K.
Electron Tube Division #2
Iwata-gun 438-0193, Japan

Shigehiro Sato
Iwate Medical University
Department of Microbiology
School of Medicine
Morioka 020-8505, Japan

Kazuyoshi Takayama, MEMBER SPIE
Tohoku University
Shock Wave Research Center
Institute of Fluid Science
Sendai 980-8577, Japan

Abstract. In the plasma flash x-ray generator, a 200-nF condenser is charged up to 50 kV by a power supply, and flash x-rays are produced by the discharging. The x-ray tube is a demountable triode with a trigger electrode, and the turbomolecular pump evacuates air from the tube with a pressure of approximately 1 mPa. Target evaporation leads to the formation of weakly ionized linear plasma, consisting of copper ions and electrons, around the fine target, and intense Kα rays are produced using a 10-μm-thick nickel filter. At a charging voltage of 50 kV, the maximum tube voltage is almost equal to the charging voltage of the main condenser, and the peak current is about 15 kA. When the charging voltage is increased, the linear plasma forms, and the copper Kα intensities substantially increase. The Kα lines are quite clean and intense, and hardly any bremsstrahlung rays are detected at all. The x-ray pulse widths are approximately 700 ns, and the time-integrated x-ray intensity has a value of approximately 20 μC/kg at 1.0 m from the x-ray source with a charging voltage of 50 kV. [DOI: 10.1117/1.1882373]

Subject terms: flash x-ray; weakly ionized linear plasma; copper target; Kα characteristic x-rays; monochromatic x-rays.

Paper 040184 received Mar. 29, 2004; revised manuscript received Sep. 9, 2004; accepted for publication Oct. 25, 2004; published online Mar. 30, 2005. This paper is a revision of a paper presented at SPIE conference on Laser-Generated and Other Laboratory X-Ray and EUV Sources, Optics, and Applications, Aug. 2003, San Diego, California. The paper presented there appears (unrefereed) in SPIE Proceedings Vol. 5196.

1 Introduction

Flash x-rays have been produced by several different methods, and various generators have been developed corresponding to specific radiographic objectives.[1–3] Currently, maximum photon energy has been increased to approximately 1 MeV using multistage Marx pulse generators[1,2] to produce hard x-rays for military studies. In soft x-ray generators,[4–7] high-intensity single generators with large capacity condensers were originally developed. Subsequently, repetitive generators[8–12] have been developed, and the repetition rate has been increased to subkilohertz using a cold-cathode triode.

Recently, soft x-ray lasers have been produced by a gas-discharge capillary,[13–16] and the laser pulse energy substantially increased in proportion to the capillary length. These kinds of fast discharges can generate hot and dense plasma columns with aspect ratios approaching 1000:1. However, it is difficult to increase the laser photon energy to 10 keV or beyond. Because there are no x-ray resonators in the high photon energy region, new methods for increasing coherence will be desired in the future.

We have developed several different plasma flash x-ray generators corresponding to specific radiographic objectives, and a major goal in our research is the development of an intense and clean monochromatic x-ray generator that can impact applications with biomedical radiography. By forming weakly ionized linear plasma,[17–20] because we have succeeded in producing fairly intense and clean quasi-monochromatic x-rays from the plasma axial direction, monochromatic x-rays should be produced using a K-edge filter.

We describe a plasma flash x-ray generator utilizing a new plasma x-ray tube, and used it to perform a preliminary experiment for generating clean monochromatic x-rays by forming a linear copper plasma cloud around a fine target.

2 Generator

2.1 *High-Voltage Circuit*

Figure 1 shows a block diagram of the high-intensity plasma flash x-ray generator. This generator consists of the following essential components: a high-voltage power supply, a high-voltage condenser with a capacity of approximately 200 nF, a turbomolecular pump, a krytron pulse

0091-3286/2005/$22.00 © 2005 SPIE

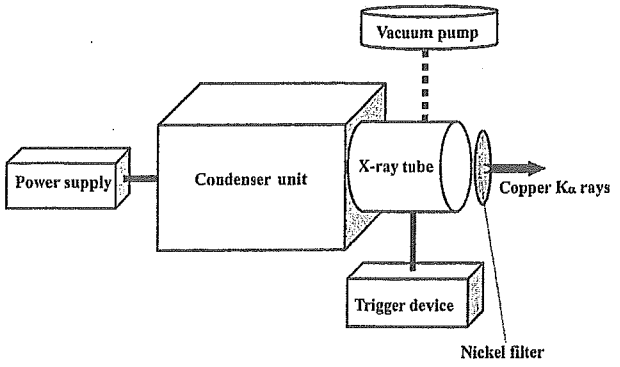

Fig. 1 Block diagram of high-intensity plasma flash x-ray generator.

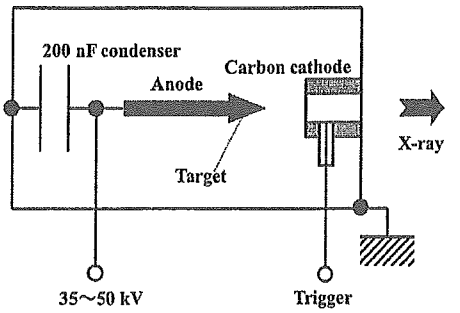

Fig. 2 Circuit diagram of generator.

generator as a trigger device, and a flash x-ray tube. In this generator, a low-impedance transmission line (Fig. 2) is employed to increase maximum tube current. The high-voltage main condenser is charged to 50 kV by the power supply, and electric charges in the condenser are discharged to the tube after triggering the cathode electrode with the trigger device. The plasma flash x-rays are then produced.

2.2 *X-Ray Tube*

The x-ray tube is a demountable cold cathode triode that is connected to the turbomolecular pump with a pressure of approximately 1 mPa (Fig. 3). This tube consists of the following major parts: a hollow cylindrical carbon cathode with a bore diameter of 10.0 mm, a brass focusing electrode, a trigger electrode made from copper wire, a stainless-steel vacuum chamber, a nylon insulator, a polyethylene terephthalate (Mylar) x-ray window 0.25 mm thick, and a rod-shaped copper target 3.0 mm in diameter with a tip angle of 60 deg. The distance between the target and cathode electrodes is approximately 20 mm, and the trigger electrode is set in the cathode electrode. As electron beams from the cathode electrode are roughly converged to the target by the focusing electrode, evaporation leads to the formation of a weakly ionized linear plasma, consisting of copper ions and electrons, around the fine target.

2.3 *Principle of Clean Kα-Ray Irradiation*

In the linear plasma, bremsstrahlung photons with energies higher than the K-absorption edge are effectively absorbed and are converted into fluorescent x-rays (Fig. 4). The plasma then transmits the fluorescent rays easily, and bremsstrahlung rays with energies lower than the K edge are also absorbed by the plasma. In addition, because bremsstrahlung rays are not emitted in the opposite direction to that of electron acceleration, intense characteristic x-rays are generated from the plasma-axial direction. Sub-

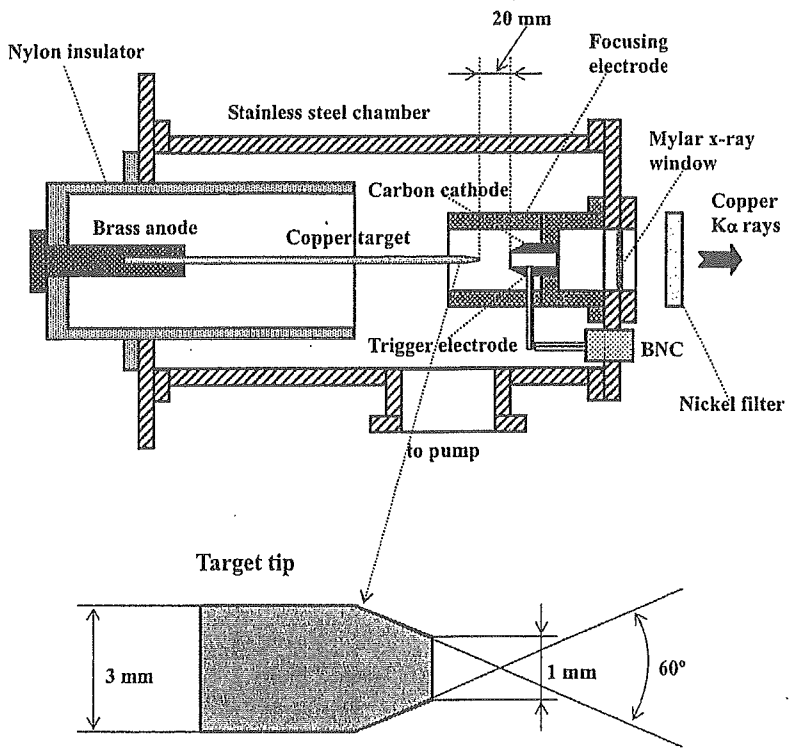

Fig. 3 Schematic drawing of flash x-ray tube with rod target.

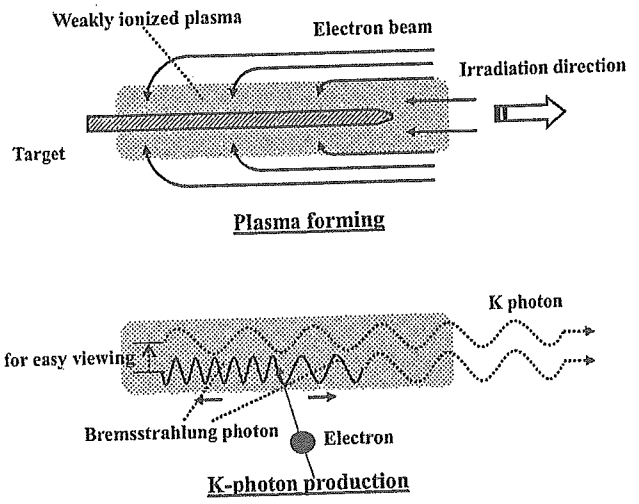

Fig. 4 K-photon irradiation from weakly ionized plasma.

sequently, Kβ rays (8.90 keV) are absorbed effectively using a 10-μm-thick nickel K-edge filter with an edge of 8.33 keV, and quite clean Kα rays (8.04 keV) are produced.

3 Characteristics

3.1 *Tube Voltage and Current*

Tube voltage and current were measured by a high-voltage divider with an input impedance of 1 GΩ and a current transformer, respectively. Figure 5 shows the time relation for the tube voltage and current. At the indicated charging voltages, they roughly displayed damped oscillations. When the charging voltage was increased, both the maximum tube voltage and current increased. At a charging voltage of 50 kV, the maximum tube voltage was almost equal to the charging voltage of the main condenser, and the maximum tube current was approximately 15 kA.

3.2 *X-Ray Output*

An x-ray output pulse was detected using a combination of a plastic scintillator and a photomultiplier using a 10-μm-thick monochromatic copper filter (Fig. 6). The x-ray pulse height substantially increased with corresponding increases in the charging voltage. The x-ray pulse widths were about 700 ns, and the time-integrated x-ray intensity per pulse measured by a thermoluminescence dosimeter (Kyokko TLD Reader 1500 utilizing MSO-S elements without energy compensation) had a value of about 20 μC/kg at 1.0 m from the x-ray source, with a charging voltage of 50 kV.

3.3 *X-Ray Source*

To measure images of the Kα source, we employed a pinhole camera with a hole diameter of 100 μm (Fig. 7). When the charging voltage was increased, the plasma x-ray source grew, and both spot dimension and intensity increased. Because the x-ray intensity is the highest at the center of the spot, both the dimension and intensity decreased according to both increases in the thickness of a filter for absorbing x-rays and decreases in the pinhole diameter.

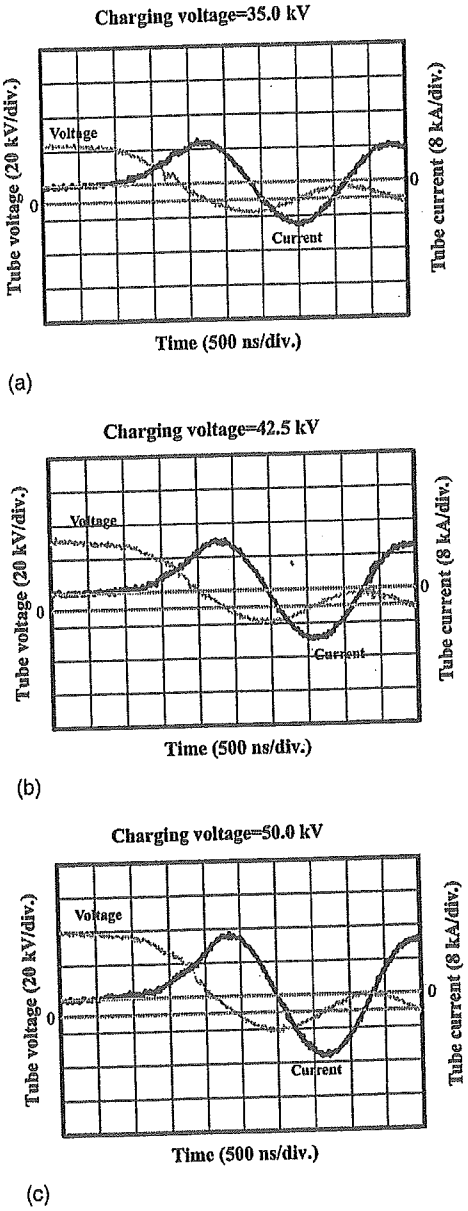

Fig. 5 Tube voltages and currents with charging voltage of (a) 35.0 kV, (b) 42.5 kV, and (c) 50.0 kV.

3.4 *X-Ray Spectra*

X-ray spectra from the plasma source were measured using a transmission-type spectrometer with a lithium fluoride

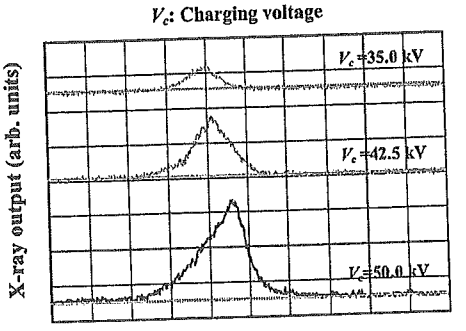

Fig. 6 X-ray outputs measured by plastic scintillator with changes in charging voltage.

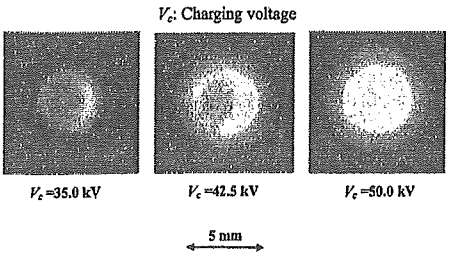

Fig. 7 Images of Kα x-ray source measured by pinhole of 100 μm from plasma axial direction.

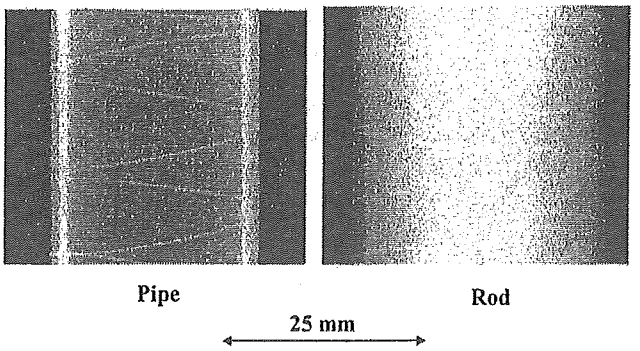

Fig. 9 Radiograms of tungsten wires 50 μm in diameter coiled around pipe, and rod made of polymethyl methacrylate.

curved crystal 0.5 mm in thickness. The spectra were taken by a computed radiography (CR) system[21] (Konica Regius 150) with a wide dynamic range, using the filter, and relative x-ray intensity was calculated from Dicom digital data. Figure 8 shows measured spectra from the copper target using the filter. In fact, we observed clean Kα lines such as lasers, and confirmed the significant filtering effect, while bremsstrahlung rays were hardly detected at all. The characteristic x-ray intensity of the Kα lines substantially increased with corresponding increases in the charging voltage, and the Kβ line was absorbed by the filter. Although this spectrometer has sufficient energy resolution for measuring Kα_1 and Kα_2 lines, we could observe only a single line.

4 Radiography

Plasma radiography was performed by the CR system without using the filter, and the distance between the x-ray source and imaging plate was 1.2 m.

First, rough measurements of image resolution were made using wires. Figure 9 shows radiograms of 50-μm-diam tungsten wires coiled around a pipe, and a rod made of polymethyl methacrylate with a charging voltage of 50 kV. Although the image contrast increased using the pipe, 50-μm-diam wires could be observed.

The image of water falling into a polypropylene beaker from a glass test tube is shown in Fig. 10. This image was taken with a charging voltage of 45 kV, with the slight addition of an iodine-based contrast medium. Because the x-ray duration was about 1 μs, the stop-motion image of water could be obtained.

Figure 11 shows an angiogram of a rabbit heart; iodine-based microspheres of 15 μm in diameter were used with a charging voltage of 50 kV, and fine blood vessels of about 100 μm were visible.

5 Discussion

Concerning the spectrum measurement, we obtained fairly clean Kα lines from a weakly ionized linear plasma x-ray

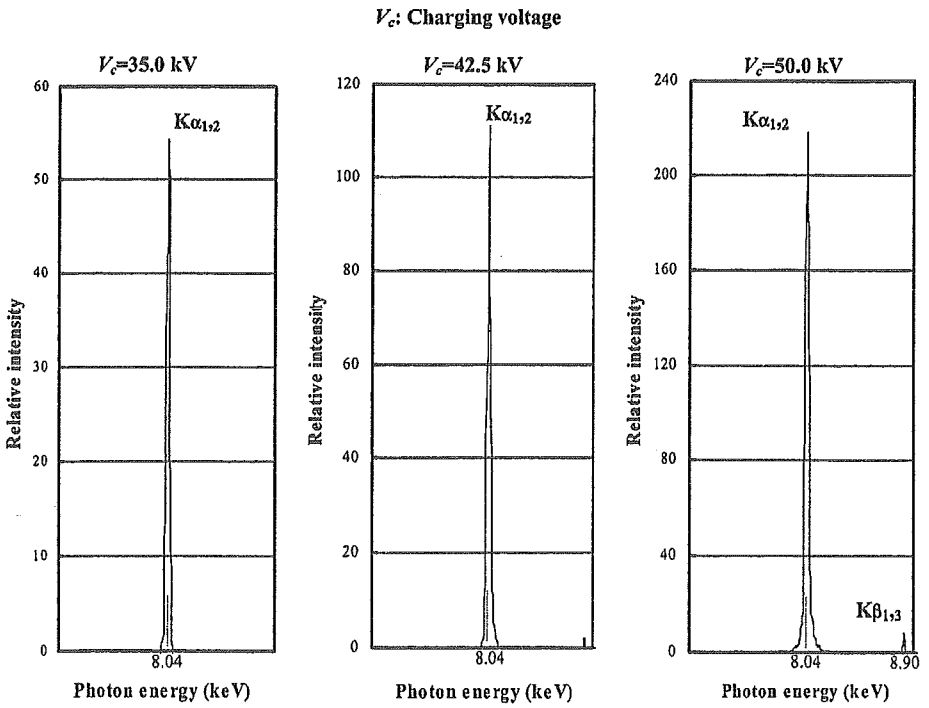

Fig. 8 X-ray spectra from weakly ionized copper plasma according to changes in charging voltage and to insertion of nickel K-edge filter.

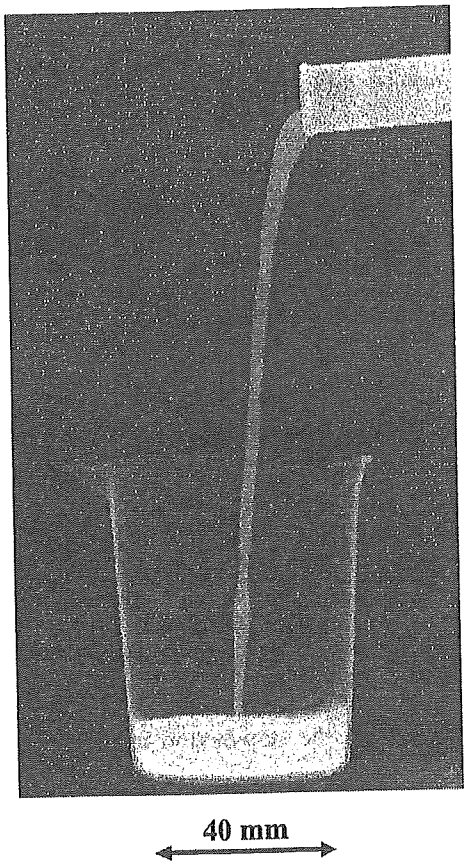

Fig. 10 Radiogram of water falling into polypropylene beaker from glass test tube.

source by absorbing Kβ lines using the K-edge filter. The lines are produced by x-ray enhancement by spontaneous emission, and the coherence can be increased by development of a resonator or by pulse laser irradiations from the plasma axial direction to produce higher harmonics. In a medical application, cerium Kα rays (34.6 keV) are absorbed effectively by an iodine-based contrast medium, and high contrast microangiography can be performed.

In this research, we obtained sufficient characteristic x-ray intensity per pulse for CR radiography using the filter, and the generator-produced number of characteristic Kα photons was approximately 5×10^{13} photons/cm$^2\cdot$s at 1.0 m from the source. In addition, since the photon energy of characteristic x-rays can be controlled by changing the target elements, various quasimonochromatic high-speed radiographies, such as high-contrast microangiography and parallel radiography using an x-ray lens, will be possible.

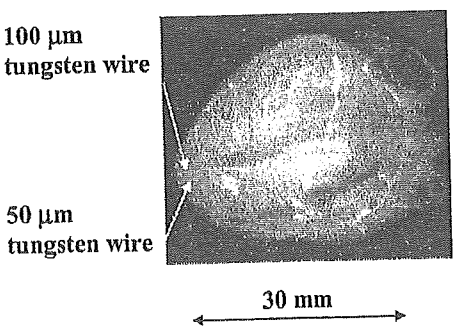

Fig. 11 Angiograms of rabbit heart.

Acknowledgments

This work was supported by Grants-in-Aid for Scientific Research (13470154, 13877114, and 16591222) and Advanced Medical Scientific Research from MECSST; Health and Labor Sciences Research Grants (RAMT-nano-001, RHGTEFB-genome-005, and RHGTEFB-saisei-003); and grants from Keiryo Research Foundation, The Promotion and Mutual Aid Corporation for Private Schools of Japan, Japan Science and Technology Agency (JST), and New Energy and Industrial Technology Development Organization (NEDO, Industrial Technology Research Grant Program in 2003).

References

1. A. Mattsson, "Some characteristics of a 600 kV flash x-ray tube," *Phys. Scr.* **5**, 99–102 (1972).
2. R. Germer, "X-ray flash techniques," *J. Phys. E* **12**, 336–350 (1979).
3. C. Cavailler, "AIRIX—a new tool for flash radiography in detonics," *Proc. SPIE* **4183**, 23–35 (2000).
4. E. Sato, H. Isobe, and F. Hoshino, "High intensity flash x-ray apparatus for biomedical radiography," *Rev. Sci. Instrum.* **57**, 1399–1408 (1986).
5. E. Sato, M. Sagae, K. Takahashi, T. Oizumi, H. Ojima, K. Takayama, Y. Tamakawa, T. Yanagisawa, A. Fujiwara, and K. Mitoya, "High-speed soft x-ray generators in biomedicine," *Proc. SPIE* **2513**, 649–667 (1994).
6. E. Sato, M. Sagae, K. Takahashi, A. Shikoda, T. Oizumi, H. Ojima, K. Takayama, Y. Tamakawa, T. Yanagisawa, A. Fujiwara, and K. Mitoya, "Dual energy flash x-ray generator," *Proc. SPIE* **2513**, 723–735 (1994).
7. E. Sato, M. Sagae, A. Shikoda, K. Takahashi, T. Oizumi, M. Yamamoto, A. Takabe, K. Sakamaki, Y. Hayasi, H. Ojima, K. Takayama, and Y. Tamakawa, "High-speed soft x-ray techniques," *Proc. SPIE* **2869**, 937–955 (1996).
8. E. Sato, S. Kimura, S. Kawasaki, H. Isobe, K. Takahashi, Y. Tamakawa, and T. Yanagisawa, "Repetitive flash x-ray generator utilizing a simple diode with a new type of energy-selective function," *Rev. Sci. Instrum.* **61**, 2343–2348 (1990).
9. S. Kimura, E. Sato, M. Sagae, A. Shikoda, T. Oizumi, K. Takahashi, Y. Tamakawa, and T. Yanagisawa, "Disk-cathode flash x-ray tube driven by a repetitive two-stage Marx pulser," *Med. Biol. Eng. Comput.* **31**, S37–S43 (1993).
10. A. Shikoda, E. Sato, M. Sagae, T. Oizumi, Y. Tamakawa, and T. Yanagisawa, "Repetitive flash x-ray generator having a high-durability diode driven by a two-cable-type line pulser," *Rev. Sci. Instrum.* **65**, 850–856 (1994).
11. E. Sato, K. Takahashi, M. Sagae, S. Kimura, T. Oizumi, Y. Hayasi, Y. Tamakawa, and T. Yanagisawa, "Sub-kilohertz flash x-ray generator utilizing a glass-enclosed cold-cathode triode," *Med. Biol. Eng. Comput.* **32**, 289–294 (1994).
12. K. Takahashi, E. Sato, M. Sagae, T. Oizumi, Y. Tamakawa, and T. Yanagisawa, "Fundamental study on a long-duration flash x-ray generator with a surface-discharge triode," *Jpn. J. Appl. Phys.* **33**, 4146–4151 (1994).
13. J. J. Rocca, V. Shlyaptsev, F. G. Tomasel, O. D. Cortazar, D. Hartshorn, and J. L. A. Chilla, "Demonstration of a discharge pumped table-top soft x-ray laser," *Proc. Phys. Lev. Lett.* **73**, 2192–2195 (1994).
14. J. J. Rocca, D. P. Clark, J. L. A. Chilla, and V. N. Shlyaptsev, "Energy extration and achievement of the saturation limit in a discharge-pumped table-top soft x-ray amplifier," *Phys. Lev. Lett.* **77**, 1476–1479 (1996).
15. C. D. Macchietto, B. R. Benware, and J. J. Rocca, "Generation of millijoule-level soft-x-ray laser pulses at a 4-Hz repetition rate in a highly saturated tabletop capillary discharge amplifier," *Opt. Lett.* **24**, 1115–1117 (1999).
16. J. J. G. Rocca, J. L. A. Chilla, S. Sakadzic, A. Rahman, J. Filevich, E. Jankowska, E. C. Hammarsten, B. M. Luther, H. C. Kapteyn, M. Murnane, and V. N. Shlyapsev, "Advances in capillary discharge soft x-ray laser research," *Proc. SPIE* **4505**, 1–6 (2001).
17. E. Sato, Y. Suzuki, Y. Hayashi, E. Tanaka, H. Mori, T. Kawai, K. Takayama, H. Ido, and Y. Tamakawa, "High-intensity quasi-monochromatic x-ray irradiation from the linear plasma target," *Proc. SPIE* **4505**, 154–164 (2001).
18. E. Sato, Y. Hayasi, E. Tanaka, H. Mori, T. Kawai, T. Usuki, K. Sato, H. Obara, T. Ichimaru, K. Takayama, H. Ido, and Y. Tamakawa,

"Quasi-monochromatic radiography using a high-intensity quasi-x-ray laser generator," *Proc. SPIE* **4682**, 538–548 (2002).
19. E. Sato, Y. Hayasi, R. Germer, E. Tanaka, H. Mori, T. Kawai, H. Obara, T. Ichimaru, K. Takayama, and H. Ido, "Irradiation of intense characteristic x-rays from weakly ionized linear molybdenum plasma," *Jpn. J. Med. Phys.* **23**, 123–131 (2003).
20. E. Sato, Y. Hayasi, R. Germer, E. Tanaka, H. Mori, T. Kawai, T. Ichimaru, K. Takayama, and H. Ido, "Quasi-monochromatic flash x-ray generator utilizing weakly ionized linear copper plasma," *Rev. Sci. Instrum.* **74**, 5236–5240 (2003).
21. E. Sato, K. Sato, and Y. Tamakawa, "Film-less computed radiography system for high-speed Imaging," *Ann. Rep. Iwate Med. Univ. Sch. Lib. Arts Sci.* **35**, 13–23 (2000).

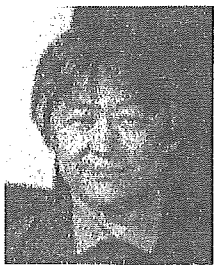

Eiichi Sato received his BS, MS, and PhD in applied physics from Tohoku Gakuin University, Sendai, Japan, in 1979, 1982, and 1987, respectively. From 1982, he was an assistant in the Department of Physics, and became as associate profrssor in 1986. Since 2004, he has been a professor of Physics at Iwate Medical University. He has written some 400 publications and delivered some 200 international presentations concerning x rays. His research interests include soft flash x-ray generators, quasi-x-ray laser generators, and high-speed radiography. In 2000 he received the Schardin Gold Medal from the German Physical Society, and in 2003 he received the Takayama Award (Gold Medal) from the Japan Society of High Speed Photography and Photonics.

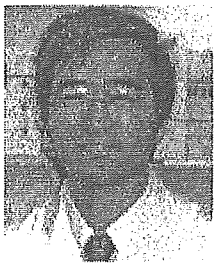

Etsuro Tanaka received his MD and PhD degrees in medicine from Kumamoto University, Japan, in 1980 and 1986, respectively. He worked on medical image processing in the Department of Physiology, Tokai University, Japan, from 1988 to 2003. He is currently a professor in the Department of Nutritional Sciences, Tokyo University of Agriculture, Japan. His research interests include medical image processing, human physiology, and clinical nutrition.

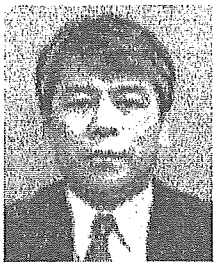

Hidezo Mori received a medical degree from Keio University School of Medicine, Tokyo, Japan, in 1977, and also a PhD from the Post Graduate School, Keio University School of Medicine. Now he is the Director of the Department of Cardiac Physiology at the National Cardiovascular Center, Suita, Japan. His primary research interests are regenerative therapy in cardiovascular disease, microcirculation, and medical applications of structural biology.

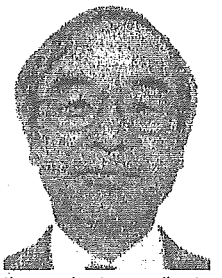

Toshiaki Kawai received the BS degree in precision mechanics and the MS degree in electronic engineering from Shizuoka University, Hamamatsu, Japan in 1964 and 1974, respectively. In 1974, he joined the Hamamatsu Photonics K.K., where he worked on research and development of solid-state infrared detectors, and then from 1978 to 1981 engaged in research work on the NEA cold cathode for application to imaging camera tubes. He is now the project coordinator of the Electron Tube Division #2 and is engaged in the development and manufacturing of imaging devices and x-ray equipment. He is a member of the Japan Radioisotope Association and the Institute of Image Information and Television Engineers of Japan.

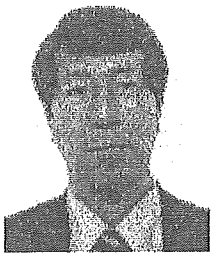

Shigehiro Sato received his MD degree from Iwate Medical University in 1980. He worked for the laboratory of the Division of Pediatric Infectious Diseases at Johns Hopkins Hospital from 1985 to 1989. He is currently a professor in the Department of Microbiology at Iwate Medical University. His research interests include central nervous system damage caused by Vero toxin, a cell culture system for vaccine development, and microangiography.

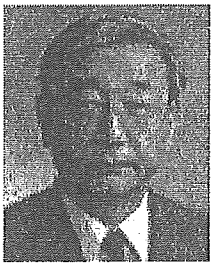

Kazuyoshi Takayama received his BS degree from Nagoya Institute of Technology in 1962. In 1970, he received his PhD in mechanical engineering from Tohoku University. Since 1986, he has been a director (professor) of the Shock Wave Research Center, Institute of Fluid Science, Tohoku University. His research interests include various shock wave phenomena, high-speed photography, and flash radiography. He has received seven awards including the coveted Ernst Mach Medal in 2000.

Acta Physiol Scand 2005, 184, 187–193

Myocardial interstitial choline and glutamate levels during acute myocardial ischaemia and local ouabain administration

T. Kawada,[1] T. Yamazaki,[2] T. Akiyama,[2] T. Shishido,[1] H. Mori[2] and M. Sugimachi[1]

1 *Department of Cardiovascular Dynamics, National Cardiovascular Center Research Institute, Osaka, Japan*

2 *Department of Cardiac Physiology, National Cardiovascular Center Research Institute, Osaka, Japan*

Received 25 November 2004, accepted 16 March 2005
Correspondence: T. Kawada, Department of Cardiovascular Dynamics, National Cardiovascular Center Research Institute, 5-7-1 Fujishirodai, Suita, Osaka 565-8565, Japan.
E-mail: torukawa@res.ncvc.go.jp

Abstract

Aim: Noradrenaline (NA) uptake transporters are known to reverse their action during acute myocardial ischaemia and to contribute to ischaemia-induced myocardial interstitial NA release. By contrast, functional roles of choline and glutamate transporters during acute myocardial ischaemia remain to be investigated. Because both transporters are driven by the normal Na^+ gradient across the plasma membrane in a similar manner to NA transporters, the loss of Na^+ gradient would affect the transporter function, which would in turn alter myocardial interstitial choline and glutamate levels. The aim of the present study was to examine the effects of acute myocardial ischaemia and the inhibition of Na^+,K^+-ATPase on myocardial interstitial glutamate and choline levels.

Methods: In anaesthetized cats, we measured myocardial interstitial glutamate and choline levels while inducing acute myocardial ischaemia or inhibiting Na^+,K^+-ATPase by local administration of ouabain.

Results: The choline level was not changed significantly by ischaemia (from 0.93 ± 0.06 to 0.82 ± 0.13 μM, mean ± SE, $n = 6$) and was decreased slightly by ouabain (from 1.30 ± 0.06 to 1.05 ± 0.07 μM, $P < 0.05$, $n = 6$). The glutamate level was significantly increased from 9.5 ± 1.9 to 34.7 ± 6.1 μM by ischaemia ($P < 0.01$, $n = 6$) and from 8.9 ± 1.0 to 15.9 ± 2.3 μM by ouabain ($P < 0.05$, $n = 6$). Inhibition of glutamate transport by *trans*-L-pyrrolidine-2,4-dicarboxylate (*t*-PDC) suppressed ischaemia- and ouabain-induced glutamate release.

Conclusion: Myocardial interstitial choline level was not increased by acute myocardial ischaemia or by Na^+,K^+-ATPase inhibition. By contrast, myocardial interstitial glutamate level was increased by both interventions. The glutamate transporter contributed to glutamate release via retrograde transport.

Keywords acetylcholine, cardiac microdialysis, cats, coronary artery occlusion, myocardium, noradrenaline.

Acute myocardial ischaemia causes oxygen depletion and loss of ATP in the ischaemic region (Hearse 1979). Blockade of H^+-ATPase leads to noradrenaline (NA) leakage from storage vesicles and axoplasmic NA accumulation (Schömig *et al.* 1988). Intracellular acidosis causes Na^+ influx via Na^+/H^+ exchange. Inhibition of Na^+,K^+-ATPase activity reduces the Na^+ gradient across the plasma membrane. Because NA uptake transporters are driven by the normal Na^+ electrochemical gradient across the plasma membrane,

axoplasmic NA accumulation and reduction of the Na^+ gradient cause reverse transport of NA from the intracellular space to the extracellular space (Schwartz 2000). Acute myocardial ischaemia evokes the myocardial interstitial NA release in the ischaemic region via retrograde NA transport, independently of efferent sympathetic nerve activity (Schömig *et al.* 1984, Yamazaki *et al.* 1996, Akiyama & Yamazaki 1999, Kawada *et al.* 2001a).

Similar to NA, choline and glutamate are taken up into cells by plasma membrane transporters driven by the Na^+ gradient (Schwartz 2000). We hypothesized that the loss of Na^+ gradient under ischaemic conditions would interfere with the transporter function, which would in turn alter myocardial interstitial choline and glutamate levels. Choline release has been suggested as an index of ischaemic degradation of the myocardial phospholipid bilayer in isolated, Tyrode solution-perfused rat hearts (Brühl *et al.* 2004). Glutamate can be a preferred myocardial fuel during ischaemia and may have protective effects on ischaemic myocardium (Arsenian 1998). Measuring myocardial interstitial levels of these molecules *in vivo* would contribute to understanding the pathophysiology of acute myocardial ischaemia. To test the hypothesis, we employed an *in vivo* cardiac microdialysis technique and measured myocardial interstitial choline and glutamate levels in anaesthetized cats (Akiyama *et al.* 1991, 1994, Yamazaki *et al.* 1997, Kawada *et al.* 2001b). Acute myocardial ischaemia inevitably affects systemic haemodynamics and perfusion of the heart. To minimize such haemodynamic effects, we also examined the effects of Na^+,K^+-ATPase inhibition on the myocardial interstitial choline and glutamate levels by locally administering ouabain through a dialysis probe (Yamazaki *et al.* 1999, Kawada *et al.* 2002). The results of the present study indicated that the myocardial interstitial choline level was not increased by acute myocardial ischaemia or by Na^+,K^+-ATPase inhibition. By contrast, the myocardial interstitial glutamate level was increased by both interventions. The glutamate transporter contributed to glutamate release via retrograde transport.

Materials and methods

Surgical preparation

Animal care was conducted in strict accordance with the *Guiding Principles for the Care and Use of Animals in the Field of Physiological Sciences* approved by the Physiological Society of Japan. Adult cats weighing 2.0–4.8 kg were anaesthetized via an intraperitoneal injection of pentobarbital sodium (30–35 mg kg^{-1}) and ventilated mechanically with room air mixed with oxygen. The depth of anaesthesia was maintained with a continuous intravenous infusion of pentobarbital sodium (1–2 mg kg^{-1} h^{-1}) through a catheter inserted via the right femoral vein. Mean systemic arterial pressure was monitored from a catheter inserted via the right femoral artery.

With the animal in the lateral position, the left fifth and sixth ribs were resected to expose the heart. When a coronary occlusion was necessary, a 3-0 silk suture was prepared around the left anterior descending coronary artery (LAD) just distal to the first diagonal branch. With a fine guiding needle, a dialysis probe was implanted into the left ventricular free wall perfused by the LAD. Heparin sodium (100 U kg^{-1} bolus injection followed by a maintenance dose of 50 U kg^{-1} h^{-1}) was administered intravenously to prevent blood coagulation. At the end of the experiment the experimental animals were killed by an overdose of pentobarbital sodium. We confirmed that the dialysis probe had been implanted within the left ventricular myocardium.

Dialysis technique

We designed a transverse dialysis probe (Akiyama *et al.* 1991, 1994). For measurements of small molecular compounds including ACh, choline, and glutamate, we used a dialysis fibre of 50 000 molecular weight cutoff (13 mm length, 310 μm OD, 200 μm ID; PAN-1200, Asahi Chemical, Osaka, Japan) with both ends glued to polyethylene tubes (20 cm length, 500 μm OD, 200 μm ID). The dialysis probe was perfused at a rate of 2 μL min^{-1} with Ringer solution. Each sample was collected in a microtube containing 3 μL of phosphate buffer (100 mM, pH 3.5). A cholinesterase inhibitor eserine (100 μM) was added to the perfusate to measure ACh. A preliminary examination indicated that whether the perfusate-contained eserine did not affect myocardial interstitial choline levels significantly. Dead space volume between the dialysis fibre and the sample microtube was identical for ACh, choline, and glutamate measurements, and the sampling was performed taking into account the time for dialysate to traverse the dead space volume.

The dialysate ACh and choline levels were measured directly by high-performance liquid chromatography with electrochemical detection. The absolute detection limits of ACh and choline, determined with a signal-to-noise ratio of 3, were 10 and 5 fmol per injection, respectively. The dialysate glutamate level was measured by kinetic enzymatic analysis with CMA 600. The absolute detection limit of glutamate was 1 μM per injection.

Protocols

All protocols were started from 2 h after implanting the dialysis probe. To examine changes in myocardial

interstitial ACh and choline levels during acute myocardial ischaemia ($n = 6$), after collecting a 15-min baseline dialysate sample, we occluded the LAD for 60 min and obtained four consecutive 15-min dialysate samples. The full-length of the implanted dialysis fibre was located within the ischaemic area judged by discolouration of myocardium during the LAD occlusion. We then released the occlusion and collected a 15-min dialysate sample during reperfusion. To examine changes in myocardial ACh and choline levels in response to local ouabain administration ($n = 6$), after collecting a 15-min baseline dialysate sample, we replaced the perfusate with Ringer solution containing 100 μM ouabain and collected four consecutive 15-min dialysate samples.

In different groups of animals, myocardial interstitial glutamate levels were measured during acute myocardial ischaemia ($n = 6$) and during local administration of ouabain ($n = 6$). To elucidate the role of the glutamate transporter, we also examined the effects of glutamate transport inhibition by *trans*-L-pyrrolidine-2,4-dicarboxylate (*t*-PDC, 10 mM) on myocardial interstitial glutamate levels during acute myocardial ischaemia ($n = 7$) and local administration of ouabain ($n = 7$). *t*-PDC was locally administered through the dialysis probe to avoid systemic effects.

Statistical analysis

All data are presented as mean ± SE values. In each protocol, the effects of myocardial ischaemia or local ouabain administration were examined using one-way analysis of variance followed by Dunnett's test against the corresponding baseline level (Glantz 2002). The baseline as well as maximum glutamate levels with and without glutamate transport inhibition were compared by an unpaired *t*-test during acute myocardial ischaemia or during local ouabain administration (Glantz 2002). Differences were considered to be significant when $P < 0.05$.

Results

Figure 1a shows myocardial interstitial ACh level during acute myocardial ischaemia. The ACh level was increased by LAD occlusion, becoming approximately 15 times higher than the baseline level at 30–45 and 45–60 min of ischaemia. The ACh level decreased towards the baseline level upon reperfusion. Figure 1b illustrates myocardial interstitial choline level during acute myocardial ischaemia. The choline level did not change significantly throughout the ischaemic and reperfusion periods.

Figure 2a shows changes in myocardial interstitial ACh level during local administration of ouabain. The ACh level was increased by the inhibition of

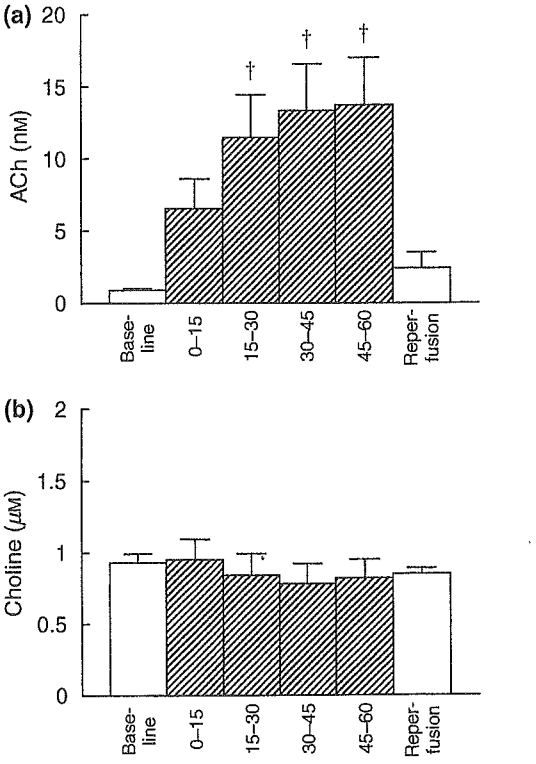

Figure 1 Changes in myocardial interstitial acetylcholine (ACh) level (a) and choline level (b) during coronary artery occlusion and reperfusion. Myocardial interstitial ACh level was significantly increased by acute myocardial ischaemia, while myocardial interstitial choline level was not changed. Data are mean ± SE. †$P < 0.01$ from baseline.

Na^+,K^+-ATPase, becoming approximately nine times higher than the baseline level at 15–30 min. The ACh level then decreased but remained significantly higher than the baseline level. Figure 2b illustrates the myocardial interstitial choline level during local administration of ouabain. The choline level was significantly lower at 0–15 and 45–60 min when compared with the baseline level.

Figure 3a shows changes in myocardial interstitial glutamate level during acute myocardial ischaemia. LAD occlusion increased the glutamate level to approximately 3.5 times higher than the baseline level at 0–15 min. Thereafter, the glutamate level was significantly higher than the baseline level throughout the ischaemic and reperfusion periods. Figure 3b illustrates the effects of glutamate transport inhibition on the ischaemia-induced glutamate release. The baseline glutamate level was significantly decreased by glutamate transport inhibition ($P < 0.05$). Although acute myocardial ischaemia and reperfusion significantly increased the glutamate level relative to the baseline level, the maximum glutamate level was attenuated to approximately one-fifth compared with that observed without glutamate transport inhibition ($P < 0.05$).

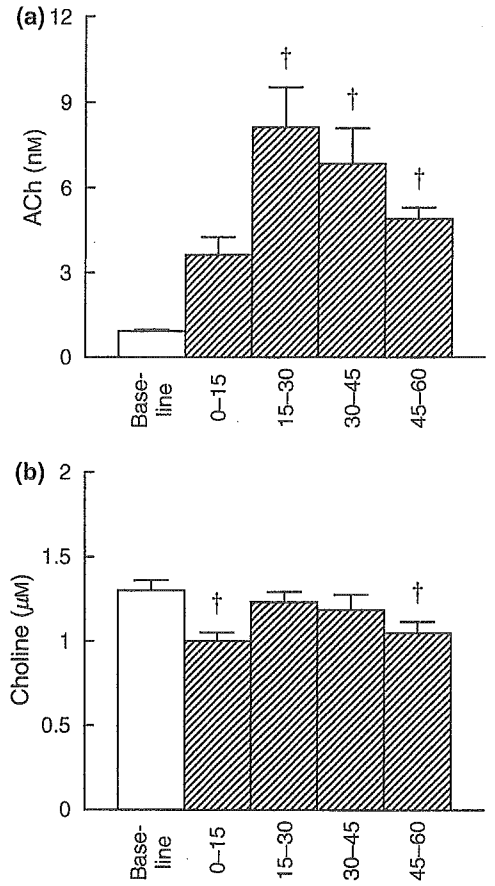

Figure 2 Changes in myocardial interstitial acetylcholine (ACh) level (a) and choline level (b) in response to the local administration of ouabain. Myocardial interstitial ACh level was significantly increased by ouabain. In contrast, myocardial interstitial choline level was decreased by ouabain. Data are mean ± SE. †$P < 0.01$ from baseline.

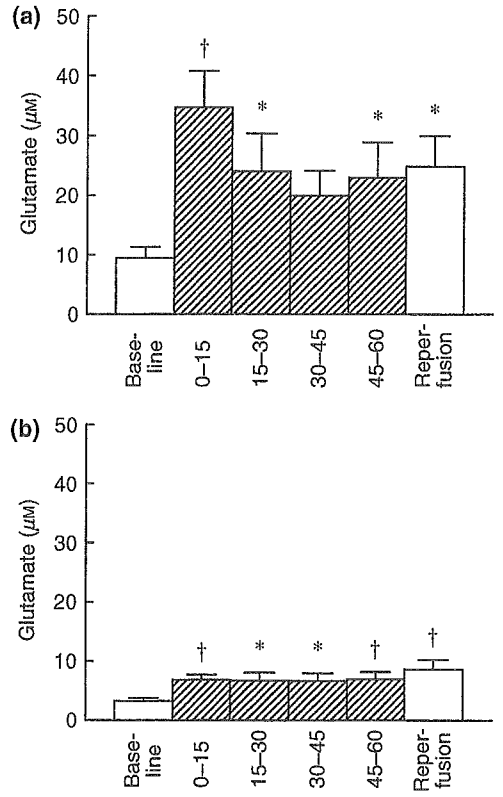

Figure 3 Changes in myocardial interstitial glutamate level during coronary artery occlusion and reperfusion without (a) and with (b) the inhibition of glutamate transporter. The glutamate level was significantly increased by acute myocardial ischaemia. The ischaemia-induced glutamate release was suppressed by the inhibition of glutamate transporter. Data are mean ± SE. †$P < 0.01$ and *$P < 0.05$ from baseline.

Figure 4a shows changes in myocardial interstitial glutamate level during the local administration of ouabain. Ouabain administration did not change the glutamate level at 0–15 min but increased the glutamate level thereafter. The glutamate level became approximately 1.8 times higher than the baseline level at 30–45 min. Figure 4b illustrates the effects of glutamate transport inhibition on ouabain-induced glutamate release. The baseline glutamate level was significantly decreased by the inhibition of glutamate transport ($P < 0.05$). Although ouabain administration increased the glutamate level relative to the baseline level, the maximum glutamate level was suppressed to approximately one-third of that observed without glutamate transport inhibition ($P < 0.05$).

Discussion

We have shown that acute myocardial ischaemia and local inhibition of Na^+,K^+-ATPase increased myocardial interstitial glutamate level but not choline level. Despite the similar Na^+ gradient dependency of corresponding transporters, myocardial interstitial glutamate and choline levels showed differential responses to the two interventions.

Changes in myocardial interstitial choline level

In the vagal nerve endings, ACh is hydrolysed to acetate and choline by acetylcholinesterase (Nicholls 1994). Choline is then taken up into the vagal nerve endings by the choline transporter driven by the Na^+ gradient. We hypothesized that loss of Na^+ gradient during acute myocardial ischaemia or local ouabain administration would increase the myocardial interstitial choline level by the interruption of choline uptake. Contrary to our hypothesis, acute myocardial ischaemia did not change myocardial interstitial choline level in the ischaemic region (Fig. 1b). Ouabain administration decreased the myocardial interstitial choline level at 0–15 and 45–60 min (Fig. 2b).

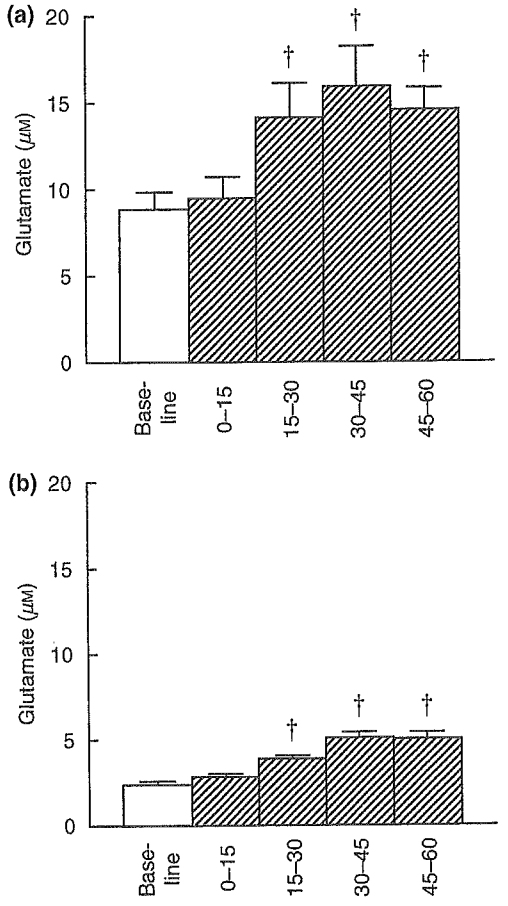

Figure 4 Changes in myocardial interstitial glutamate level in response to the local administration of ouabain without (a) and with (b) the inhibition of glutamate transporter. The glutamate level was significantly increased by ouabain administration. The ouabain-induced glutamate release was suppressed by the inhibition of glutamate transporter. Data are mean ± SE. †$P < 0.01$ from baseline.

Possible explanations for the absence of ischaemia- or ouabain-induced choline release are as follows. First, choline uptake is the rate-limiting step for ACh synthesis (Lockman & Allen 2002). Because choline in the intracellular space is rapidly consumed for ACh synthesis, the axoplasmic choline concentration might have been too low to evoke reverse transport by the choline transporter. Second, plasma choline concentration is stabilized by *de novo* choline synthesis from the catabolism of phosphatidylcholine found in cell membranes (Lockman & Allen 2002). Potential choline release may have been counterbalanced by the local stabilization mechanisms. Taking into account the recovery rate of the dialysis probe (approximately 30%), the myocardial interstitial choline concentration was 3–5 μM. Although the estimated concentration was lower than the highly regulated plasma choline concentration of approximately 10 μM, it was much higher than the ischaemia-induced maximum choline release (approximately 0.6 μM) in isolated rat hearts reported by Brühl *et al.* (2004). The present results suggest that myocardial interstitial choline level may not serve as an indicator of myocardial ischaemia in blood-perfused *in vivo* feline hearts.

By contrast with myocardial interstitial choline level, myocardial interstitial ACh level was increased both by acute myocardial ischaemia and by local administration of ouabain. Because ischaemia-induced ACh release was observed after vagal nerve transection in a previous study (Kawada *et al.* 2000), a Ca^{2+} channel-independent, regional release mechanism appears to be involved. Several reports have suggested that ouabain or ischaemia-induced intracellular Na^+ accumulation could elevate intracellular Ca^{2+} level via Na^+/Ca^{2+} exchange (Mochizuki & Jiang 1998, Li *et al.* 2000). The elevation of intracellular Ca^{2+} level may be associated with ACh release. Our previous study indicated that intracellular Ca^{2+} overload due to Ca^{2+} mobilization is responsible for the ACh release evoked by ischaemia (Kawada *et al.* 2000).

Changes in myocardial interstitial glutamate levels

Although the glutamate transporter family differs from the NA transporter family in that it requires counter-transport of K^+ instead of cotransport of Cl^-, its primary driving force is the Na^+ gradient across the plasma membrane (Schwartz 2000). Therefore, interventions that reduce the Na^+ gradient are likely to cause reverse transport of glutamate, in a similar manner to the reverse transport of NA. Acute myocardial ischaemia increased the myocardial interstitial glutamate level (Fig. 3a) as consistent with previous reports (Kennergren *et al.* 1997, 1999, Bäckström *et al.* 2003, Song *et al.* 1996). Inhibition of Na^+,K^+-ATPase also induced myocardial interstitial glutamate release (Fig. 4a). Glutamate release during acute myocardial ischaemia and local ouabain administration was significantly attenuated by the inhibition of glutamate transport (Figs 3b and 4b), suggesting the involvement of reverse transport by the glutamate transporter. Glutamate plays a vital role in keeping nitrogen balance in cells as a common amino acid in transamination reactions. The high intra-to-extracellular concentration ratio of glutamate would contribute to the retrograde transport by the glutamate transporter during the loss of normal Na^+ gradient.

In the case of myocardial interstitial NA levels, local blockade of NA uptake increased baseline NA levels, suggesting the accumulation of NA spontaneously released into the synaptic cleft (Akiyama & Yamazaki 1999). We therefore predicted that the inhibition of glutamate transport would increase the baseline gluta-

mate level. However, the inhibition of glutamate transport actually decreased the baseline glutamate level (Figs 3 and 4), suggesting that spontaneous glutamate release rather than glutamate uptake had occurred under baseline conditions. The insertion of a dialysis probe inevitably damages the myocardium. Although we waited for 2 h after implantation of the dialysis probe and the glutamate level declined with time, glutamate release from damaged myocardium may have continued. Notwithstanding this limitation, we were able to detect glutamate release in response to acute myocardial ischaemia and inhibition of Na^+,K^+-ATPase. Therefore, our interpretation that glutamate release was dependent on the reverse transport of glutamate transporter may be reasonable.

Supplementing the heart with glutamate has been shown to have beneficial effect on the recovery of contractile function in post-surgical patients (Arsenian 1998). The myocardial interstitial glutamate level remained increased during 15-min reperfusion whereas the myocardial interstitial ACh level returned towards the baseline level. Although the reason for different responses upon reperfusion was unanswered in the present study, the sustained increase in the glutamate level may have therapeutic effect on its own.

In conclusion, acute myocardial ischaemia and inhibition of Na^+,K^+-ATPase did not increase myocardial interstitial choline level despite a significant increase in myocardial interstitial ACh level. By contrast, both interventions significantly increased the myocardial interstitial glutamate level. The glutamate transporter contributed to myocardial interstitial glutamate release via retrograde transport.

This study was supported by Health and Labour Sciences Research Grant for Research on Advanced Medical Technology (H14-Nano-002) from the Ministry of Health Labour and Welfare of Japan, by Grant-in-Aid for Scientific Research (C-15590786) from the Ministry of Education, Science, Sports and Culture of Japan, and by the Program for Promotion of Fundamental Studies in Health Science of the Organization for Pharmaceutical Safety and Research from Pharmaceuticals and Medical Devices Agency (PMDA).

References

Akiyama, T. & Yamazaki, T. 1999. Norepinephrine release from cardiac sympathetic nerve endings in the in vivo ischemic region. *J Cardiovasc Pharmacol* 34(Suppl. 4), S11–S14.

Akiyama, T., Yamazaki, T. & Ninomiya, I. 1991. In vivo monitoring of myocardial interstitial norepinephrine by dialysis technique. *Am J Physiol Heart Circ Physiol* 261, H1643–H1647.

Akiyama, T., Yamazaki, T. & Ninomiya, I. 1994. In vivo detection of endogenous acetylcholine release in cat ventricles. *Am J Physiol Heart Circ Physiol* 266, H854–H860.

Arsenian, M. 1998. Potential cardiovascular applications of glutamate, aspartate, and other amino acids. *Clin Cardiol* 21, 620–624.

Bäckström, T., Goiny, M., Lockowandt, U., Liska, J. & Franco-Cereceda, A. 2003. Cardiac outflow of amino acids and purines during myocardial ischemia and reperfusion. *J Appl Physiol* 94, 1122–1128.

Brühl, A., Hafner, G. & Löffelholz, K. 2004. Release of choline in the isolated heart, an indicator of ischemic phospholipid degradation and its protection by ischemic preconditioning: no evidence for a role of phospholipase D. *Life Sci* 75, 1609–1620.

Glantz, S.A. 2002. *Primer of Biostatistics*, 5th edn. McGraw-Hill, New York.

Hearse, D.J. 1979. Oxygen deprivation and early myocardial contractile failure: a reassessment of the possible role of adenosine triphosphate. *Am J Cardiol* 44, 1115–1121.

Kawada, T., Yamazaki, T., Akiyama, T. *et al.* 2000. Differential acetylcholine release mechanisms in the ischemic and non-ischemic myocardium. *J Mol Cell Cardiol* 32, 405–414.

Kawada, T., Yamazaki, T., Akiyama, T. *et al.* 2001a. Vagosympathetic interactions in ischemia-induced myocardial norepinephrine and acetylcholine release. *Am J Physiol Heart Circ Physiol* 280, H216–H221.

Kawada, T., Yamazaki, T., Akiyama, T. *et al.* 2001b. In vivo assessment of acetylcholine-releasing function at cardiac vagal nerve terminals. *Am J Physiol Heart Circ Physiol* 281, H139–H145.

Kawada, T., Yamazaki, T., Akiyama, T. *et al.* 2002. Disruption of vagal efferent axon and nerve terminal function in the postischemic myocardium. *Am J Physiol Heart Circ Physiol* 283, H2687–H2691.

Kennergren, C., Nyström, B., Nyström, U. *et al.* 1997. In situ detection of myocardial infarction in pig by measurements of aspartate aminotransferase (ASAT) activity in the interstitial fluid. *Scand Cardiovasc J* 31, 343–349.

Kennergren, C., Mantovani, V., Lönnroth, P., Nyström, B., Berglin, E. & Hamberger, A. 1999. Extracellular amino acids as markers of myocardial ischemia during cardioplegic heart arrest. *Cardiology* 91, 31–40.

Li, S., Jiang, Q., Stys, P.K. 2000. Important role of reverse Na^+-Ca^{2+} exchange in spinal cord white matter injury at physiological temperature. *J Neurophysiol* 84, 1116–1119.

Lockman, P.R. & Allen, D.D. 2002. The transport of choline. *Drug Dev Ind Pharm* 28, 749–771.

Mochizuki, S. & Jiang, C. 1998. Na^+/Ca^{++} exchanger and myocardial ischemia/reperfusion. *Jpn Heart J* 39, 707–714.

Nicholls, D.G. 1994. *Proteins, Transmitters and Synapses*, pp. 186–199. Blackwell Science, London.

Schömig, A., Dart, A.M., Dietz, R., Mayer, E. & Kübler, W. 1984. Release of endogenous catecholamines in the ischemic myocardium of the rat. Part A: Locally mediated release. *Circ Res* 55, 689–701.

Schömig, A., Kurz, T., Richardt, G. & Schömig, E. 1988. Neuronal sodium homeostasis and axoplasmic amine concentration determine calcium-independent noradrenaline release in normoxic and ischemic rat heart. *Circ Res* 63, 214–226.

Schwartz, J.H. 2000. Neurotransmitters. In: E.R. Kandel, J.H. Schwartz & T.M. Jessell (eds) *Principles of Neural Science*, 4th edn, pp. 280–297. McGraw-Hill, New York.

Song, D., O'Regan, M.H. & Phillis, J.W. 1996. Release of the excitotoxic amino acids, glutamate and aspartate, from the isolated ischemic/anoxic rat heart. *Neurosci Lett* 220, 1–4.

Yamazaki, T., Akiyama, T., Kitagawa, H., Takauchi, Y. & Kawada, T. 1996. Elevation of either axoplasmic norepinephrine or sodium level induced release of norepinephrine from cardiac sympathetic nerve terminals. *Brain Res* 737, 343–346.

Yamazaki, T., Akiyama, T., Kitagawa, H., Takauchi, Y., Kawada, T. & Sunagawa, K. 1997. A new, concise dialysis approach to assessment of cardiac sympathetic nerve terminal abnormalities. *Am J Physiol Heart Circ Physiol* 272, H1182–H1187.

Yamazaki, T., Akiyama, T. & Kawada, T. 1999. Effects of ouabain on in situ cardiac sympathetic nerve endings. *Neurochem Int* 35, 439–445.

Cardiovascular Drugs and Therapy 19 33–40 2005

BASIC PHARMACOLOGY

Erythropoietin Just Before Reperfusion Reduces Both Lethal Arrhythmias and Infarct Size via the Phosphatidylinositol-3 Kinase-Dependent Pathway in Canine Hearts

Akio Hirata[1], Tetsuo Minamino[1], Hiroshi Asanuma[1], Shoji Sanada[1], Masashi Fujita[1], Osamu Tsukamoto[1], Masakatsu Wakeno[2], Masafumi Myoishi[2], Ken-ichiro Okada[1], Hidekazu Koyama[1], Kazuo Komamura[3], Seiji Takashima[1], Yoshiro Shinozaki[4], Hidezo Mori[3], Hitonobu Tomoike[3], Masatsugu Hori[1], and Masafumi Kitakaze[3]

[1]*Department of Internal Medicine and Therapeutics, Osaka University Graduate School of Medicine, Suita, Osaka, Japan;* [2]*Department of Bioregulatory Medicine, Osaka University Graduate School of Medicine, Suita, Osaka, Japan;* [3]*Cardiovascular Division of Internal Medicine, National Cardiovascular Center, Suita, Osaka, Japan;* [4]*Department of Physiological Science, Tokai University School of Medicine, Isehara, Kanagawa, Japan*

Summary. **Although recent studies suggest that erythropoietin (EPO) may reduce multiple features of the myocardial ischemia/reperfusion injury, the cellular mechanisms and the clinical implications of EPO-induced cardioprotection are still unclear. Thus, in this study, we clarified dose-dependent effects of EPO administered just before reperfusion on infarct size and the incidence of ventricular fibrillation and evaluated the involvement of the phosphatidylinositol-3 (PI3) kinase in the *in vivo* canine model. The canine left anterior descending coronary artery was occluded for 90 min followed by 6 h of reperfusion. A single intravenous administration of EPO just before reperfusion significantly reduced infarct size (high dose (1,000 IU/kg): 7.7 ± 1.6%, low dose (100 IU/kg): 22.1 ± 2.4%, control: 40.0 ± 3.6%) in a dose-dependent manner. Furthermore, the high, but not low, dose of EPO administered as a single injection significantly reduced the incidence of ventricular fibrillation during reperfusion (high dose: 0%, low dose: 40.0%, control: 50.0%). An intracoronary administration of a PI3 kinase inhibitor, wortmannin, blunted the infarct size-limiting and anti-arrhythmic effects of EPO. Low and high doses of EPO equally induced Akt phosphorylation and decreased the equivalent number of TUNEL-positive cells in the ischemic myocardium of dogs. These effects of EPO were abolished by the treatment with wortmannin. In conclusion, EPO administered just before reperfusion reduced infarct size and the incidence of ventricular fibrillation via the PI3 kinase-dependent pathway in canine hearts. EPO administration can be a realistic strategy for the treatment of acute myocardial infarction.**

Key Words. **erythropoietin, myocardial infarction, ventricular arrhythmia, phosphatidylinositol-3 kinase, ischemia-reperfusion injury, apoptosis**

Introduction

Recent studies have extended the traditional role of erythropoietin (EPO) from a mediator of erythroid maturation to one that provides protection against apoptotic cell death [1,2]. Recombinant human EPO (rhEPO) has been shown to exert marked protective effects against ischemia/reperfusion injury in rats and rabbits when rhEPO is administered at different time points [3–8]. Indeed, rhEPO reduced myocardial infarct size, enhanced recovery of left ventricular developed pressure, reduced the number of apoptotic cells, and induced the phosphorylation of Akt [3–8]. In these studies, high (1,000–5,000 IU/kg) doses of rhEPO, nearly 10 times higher than that used in anemic patients with chronic renal failure [9], have been applied. Recently, it was reported that phosphatidylinositol-3 (PI3) kinase

Address for correspondence: Tetsuo Minamino, MD, PhD, Department of Internal Medicine and Therapeutics, Osaka University Graduate School of Medicine, 2-2 Yamadaoka, Suita, Osaka 565-0871, Japan, Tel.: 81-6-6879-3635; Fax: 81-6-6879-3473; E-mail: minamino@medone.med.osaka-u.ac.jp